Rheological State Diagrams for Rough Colloids in Shear Flow

Lilian C. Hsiao,[1,*] Safa Jamali,[2] Emmanouil Glynos,[4,5] Peter F. Green,[4,†] Ronald G. Larson,[3] and Michael J. Solomon[3]
[1]*Department of Chemical and Biomolecular Engineering, North Carolina State University, Raleigh, North Carolina 27695, USA*
[2]*Department of Chemical Engineering, Massachusetts Institute of Technology, Cambridge, Massachusetts 02139, USA*
[3]*Department of Chemical Engineering, University of Michigan, Ann Arbor, Michigan 48109, USA*
[4]*Department of Material Science and Engineering, University of Michigan, Ann Arbor, Michigan 48109, USA*
[5]*Institute of Electronic Structure and Laser, Foundation for Research and Technology-Hellas, Crete 71110, Greece*
(Received 14 March 2017; revised manuscript received 27 May 2017; published 11 October 2017)

To assess the role of particle roughness in the rheological phenomena of concentrated colloidal suspensions, we develop model colloids with varying surface roughness length scales up to 10% of the particle radius. Increasing surface roughness shifts the onset of both shear thickening and dilatancy towards lower volume fractions and critical stresses. Experimental data are supported by computer simulations of spherical colloids with adjustable friction coefficients, demonstrating that a reduction in the onset stress of thickening and a sign change in the first normal stresses occur when friction competes with lubrication. In the quasi-Newtonian flow regime, roughness increases the effective packing fraction of colloids. As the shear stress increases and suspensions of rough colloids approach jamming, the first normal stresses switch signs and the critical force required to generate contacts is drastically reduced. This is likely a signature of the lubrication films giving way to roughness-induced tangential interactions that bring about load-bearing contacts in the compression axis of flow.

DOI: 10.1103/PhysRevLett.119.158001

Shear thickening is an increase in the viscosity η of a concentrated suspension of particles in a fluid as the shear stress σ or shear rate rises beyond a critical value [1]. When suspensions shear thicken at high volume fractions ϕ it is frequently accompanied by complex behavior that includes S-shaped flow curves [2,3] and slow stress decays [4]. The degree of shear thickening can range from a few fold to orders of magnitude increase in η as a function of σ. These distinctions are typically used as working definitions for continuous shear thickening (CST) and discontinuous shear thickening (DST) in the literature [5]. We define weak and strong thickening using the power β as the slope of $\log(\eta)$ plotted against $\log(\sigma)$ [6], where weak thickening occurs at $0.1 \leq \beta \leq 0.7$ and strong thickening occurs at $0.7 < \beta \leq 1.0$. These categories are convenient classifications of the magnitude of the rheological response rather than a fundamental physical transition. Shifting the value of demarcation between weak and strong thickening has no qualitative impact on the state diagrams presented.

Dilatancy is sometimes observed with strong shear thickening. Reynolds showed that a dilatant suspension expands in volume because particles cannot otherwise find direct flow paths within the confined environment [7]. This tendency to expand generates a normal thrust, and causes the first normal stress difference N_1 to switch from negative to positive values if boundaries are spherical in shape and surface tension is negligible [5]. The onset stresses for shear thickening and dilatancy do not necessarily coincide [6,8]. Similarly, a sheared suspension that freely expands in volume will not shear thicken because of the lack of a confining stress [9,10].

To date, neither hydrodynamics nor friction has successfully explained the full range of flow phenomena in concentrated suspensions. When particles are pushed into close contact at high shear rates, lubrication between the particles results in fore-aft asymmetry and the subsequent formation of hydroclusters [11,12]. A hallmark of the asymmetric flow microstructure is the negative sign of N_1 [13–15], which has been observed in experiments and simulations [13,16,17]. However, hydrodynamics theory alone cannot explain the large viscosity increase in strong thickening or positive N_1 values at high σ and ϕ. A recently proposed frictional contact model suggests that DST is a result of particles making solid-solid contact when lubrication films break [2,6,18–23]. However, numerical simulations of this model consistently predict positive N_1 values regardless of the flow conditions or the particle loading [24].

The reasons for discrepancies between theory, simulations, and experiments are unclear, especially when particles are neither spherical nor smooth. In this Letter, we seek to resolve these contradictions by systematically tuning the roughness of model colloids, investigating their η and N_1 under shear, and demonstrating how surface roughness influences the macroscopic response of the suspension. Here, a rough particle has spherical symmetry and surface topography that deviates from an ideal smooth sphere by $<10\%$ of the radius. Few studies relate particle surface roughness to frictional effects in flow. One such study investigated the rheology of smooth and etched silica particles in a narrow range of volume fractions ($0.41 \leq \phi \leq 0.48$) [25]. The authors found that the onset stress for suspensions of etched silica is reduced when compared to

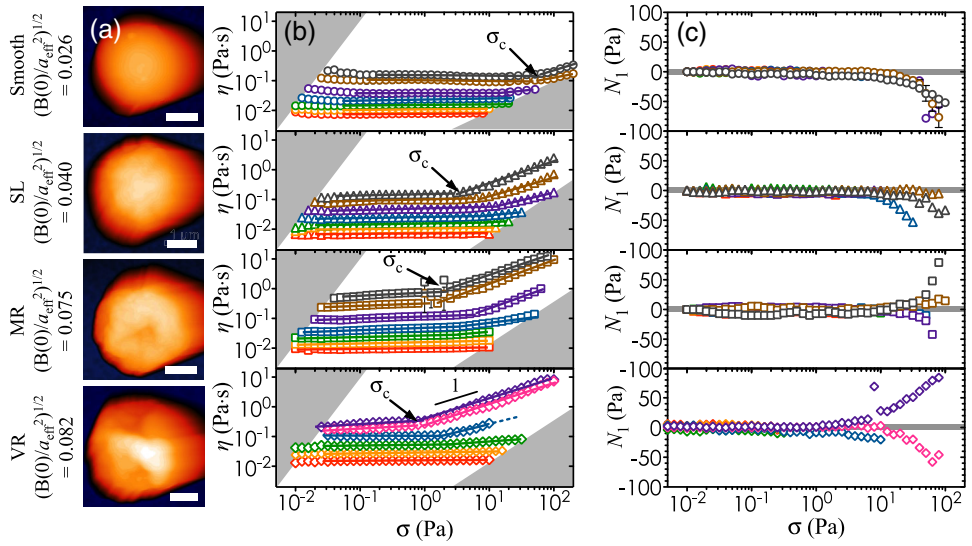

FIG. 1. Effect of particle roughness on suspension rheology. (a) Atomic force microscopy images of (left to right): smooth, SL, MR, and VR colloids. Scale bars = 1 μm. (b), (c) Flow curves of suspensions consisting of smooth, SL, MR, and VR colloids (top to bottom). Colors represent volume fractions ($\phi = 0.30$, red; $\phi = 0.35$, orange; $\phi = 0.40$, green; $\phi = 0.45$, blue; $\phi = 0.48$, pink; $\phi = 0.50$, purple; $\phi = 0.535$, brown; $\phi = 0.55$, gray). Solid lines are power law fits to the data. The data for VR colloids at $\phi = 0.45$ represent a limited stress range; a dashed line is extrapolated for visibility. Gray regions in (b) indicate instrument sensitivity limits on the left and inertial/fracture effects on the right, and gray regions in (c) centered about $N_1 = 0$ Pa indicate instrument limits. Error bars, where available, represent standard deviations from three independent upward stress sweeps.

smooth particles, and that N_1 switches signs from negative to positive. Although this result is in qualitative agreement with our work, their measured viscosities were higher than expected for near hard sphere silica colloids [26], and diverged for etched particles (roughness to particle diameter ratio = 0.6%) at a value of ϕ_{max} that is much lower than the maximum packing expected for frictional particles ($\phi_{max} = 0.54$ [2]). We aim to present a general framework that is relevant to colloids with shape anisotropy. Our results show that lubrication is dominant in moderately concentrated suspensions. Tangential interactions become more important at high shear rates, volume fractions, and surface roughness. A key observation is that the onset stress for shear thickening is independent of ϕ only in the case of smooth particles, and that roughness decreases this onset stress by reducing the force required to push colloids into contact. We present the findings as a set of rheological state diagrams that provide insight into the transition from shear thickening to dilatant flow for colloidal suspensions.

We use density and refractive index-matched dispersions that contain poly(methyl methacrylate) (PMMA) colloids with diameters $2a$ ranging from 1.9–2.8 μm [27–30], for which flow occurs without inertia. The continuum phase is an organic solvent designed to minimize sedimentation and van der Waals forces. A 10-nm layer of poly(12-hydroxystearic acid) (PHSA) copolymer is grafted onto the colloids to provide a short-range repulsive barrier against irreversible adhesion [28]. This steric stabilizer determines the range and strength of the nearly hard sphere interactions of the colloids. Experimental and numerical studies show that short-range steric stabilizers do not significantly alter the strength of the shear thickening or dilatancy unless the solvent quality is drastically changed [31–34]. Roughness of the colloids is tuned by varying the concentration of a crosslinker. The crosslinker induces heterogeneity during oligomer precipitation, resulting in size-monodisperse rough particles (Fig. S1, Table S1 in the Supplemental Material [35]) [36]. Using this method, we synthesize PMMA colloids with four types of asperities: smooth, slightly rough (SL), medium rough (MR), and very rough (VR). These categories refer to particles with different root-mean-square (rms) roughness characterized using an atomic force microscope (AFM) in tapping mode [Fig. 1(a)]. The grafting length of the PHSA brush is between 9% (VR colloids) to 50% (smooth colloids) of the rms roughness. The measured topography is fitted to a sphere with an effective radius, a_{eff}. The deviation of surface profiles from a_{eff} is minimized by least squares fittings (Fig. S2 [35]). Volume fractions are computed using a_{eff} values and from image volumes of particle suspensions captured using confocal laser scanning microscopy (CLSM) [37]. We apply the relation $\phi = 4\pi a_{eff}^3 N_p/(3V_{box})$, where N_p is the total number of particles found in V_{box}, the total volume of the CLSM image box analyzed. Our method of weighing particles and solvent yields the correct value of ϕ to 2% (Fig. S3 [35]). An additional uncertainty in ϕ of 2% is present due to particles swelling over time (Fig. S4 [35]). We characterize roughness using the autocovariance of the topographic profile [38], $B(\Psi) = (1/N)\sum_{i,j=1}^{\Psi}(|\mathbf{r}_i| - a_{eff})(|\mathbf{r}_j| - a_{eff})$, where N is the total number of data points analyzed and $\Psi = \cos^{-1}(\mathbf{r}_i \cdot \mathbf{r}_j/|\mathbf{r}_i||\mathbf{r}_j|)$ is the angle between $\mathbf{r}_i$ and $\mathbf{r}_j$ as defined in Fig. S2d in the Supplemental Material [35]. The relative rms roughness is expressed as $[B(\psi = 0)/a_{eff}^2]^{1/2}$ to account for

different particle sizes. The full range of our experimental conditions is in Table S2 [35].

Colloids with large surface roughness shear thicken more readily. When vials containing suspensions at $\phi = 0.52$ are inverted, smooth colloids flow like a viscous fluid whereas rough colloids form fingerlike structures (Fig. S2, Movie S1 [35]). To quantify the shear thickening as a function of roughness and ϕ, we measure η and N_1 as a function of σ in a stress-controlled rheometer. Performing stress sweeps up and down shows that the flow is completely reversible for smooth colloids at $\phi = 0.55$, whereas MR colloids show hysteresis in η and N_1 at $\phi = 0.535$ when steady state flow conditions are imposed (Fig. S5 [35]). The hysteresis could be from geometric friction caused by interlocking particles during flow. We also verify the absence of global slip by comparing the flow curve of MR colloids with that collected with a different cone-and-plate geometry (Fig. S6 [35]).

Figure 1 shows the flow curves of the colloidal suspensions. At low σ, the suspensions flow with a nearly constant relative viscosity, $\eta_{r,N}$, defined as the quasi-Newtonian plateau past the zero shear viscosity and the shear thinning regime [15]. As σ increases, η begins to increase significantly at the onset of shear thickening. The critical onset stress, σ_c, is the intersection of power laws fitted to the quasi-Newtonian and shear thickening regimes [Fig. 1(b)]. Smooth colloids undergo weak thickening in the range of ϕ tested. A progression towards strong thickening is seen when surface roughness increases. Although σ_c is independent of ϕ for smooth colloids, σ_c decreases with increasing ϕ for SL, MR, and VR colloids. These observations are markedly different from multiple studies, which show that σ_c is typically constant in both regimes of CST and DST [6,21,39]. We address the rationale for the difference between smooth and rough particles later.

The sign of N_1 changes from negative to positive at large σ in strong thickening, indicating the presence of dilatancy. Our measurements show that smooth colloids display negative N_1 values consistently, whereas increasing the rms roughness causes the sign change to occur at lower ϕ for MR ($\phi = 0.535$, 0.55) and VR colloids ($\phi = 0.50$) [Fig. 1(c)]. Previous studies have attributed negative N_1 values and a mild increase in η to the formation of hydroclusters [13]. More recently, positive N_1 values are attributed to a breakdown of lubrication films [6,18]. Here, our simulations support our inference that roughness shifts the shear thickening-dilatancy transition because of an increase in the interparticle friction coefficient, μ. Figures 2(a) and 2(b) show results of dissipative particle dynamics (DPD) simulations [16] on a suspension of spherical particles ($\phi = 0.535$) with adjustable tangential interactions ranging from frictionless ($\mu = 0$) to frictional ($\mu = 1$). The simulations utilize both lubrication hydrodynamics and friction to support experimental observations that dilatancy and strong thickening are caused by tangential interactions from particle asperities.

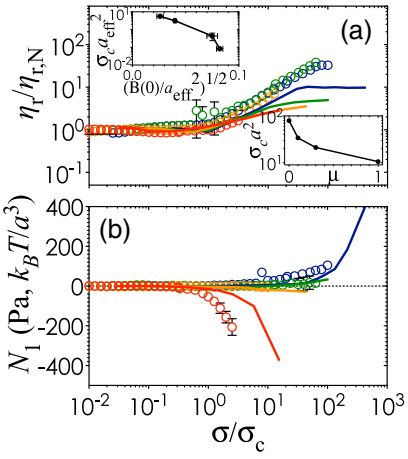

FIG. 2. Simulations and experiments of frictionless (smooth) and frictional (rough) particles. (a) Normalized steady state viscosity and (b) N_1 values of colloidal suspensions. Both plots are generated for $\phi = 0.535$ (except for VR colloids plotted at $\phi = 0.50$). Data from experiments are plotted as open circles for four types of roughness (smooth, red; SL, orange; MR, green; VR, blue) and data from DPD simulations are plotted as solid lines for DPD particles with varying friction coefficients ($\mu = 0$, red; $\mu = 0.1$, orange; $\mu = 0.3$, green; $\mu = 1$, blue). (Inset in a) The critical onset stress as a function of roughness in experiments and as a function of μ in DPD simulations. Error bars represent standard deviations from three independent measurements.

Two main points can be taken from Fig. 2. First, σ_c shifts to lower values as μ and roughness increase [Figs. 2(a), Inset]. This observation qualitatively supports our hypothesis that particle roughness is directly connected to friction. Since the critical onset stress is related to the pairwise force balance, this also suggests that tangential interactions reduce the critical force required to push particles into load-bearing contact. Second, there is a corresponding change in N_1 from negative to positive values as μ increases beyond a critical value. This sign change occurs only when tangential interactions are significant compared to hydrodynamics. We note that the value of σ_c does not correspond to the onset stress of dilatancy.

A natural follow-up question is: how does roughness contribute to the mechanism of the flow transitions? To address this question, we analyze the quasi-Newtonian viscosity, the shear thickening power, and the onset stresses as functions of roughness. Figure 3(a) shows that $\eta_{r,N}$ diverges more rapidly with increasing ϕ for rougher particles. Our data fit well to the empirical Eilers model $\eta_{r,N} = [1 + 1.5(1\text{-}\phi/\phi_{max})^{-1}]^2$, where ϕ_{max} is the volume fraction at which the viscosity diverges [40,41]. The $\eta_{r,N}$ data for smooth and SL colloids fall within the spread measured in previous works [21,26,42,43], whereas MR and VR colloids differ significantly. This is not due to uncertainties in ϕ for the rough colloids (Fig. S3 [35]). Their lower values of ϕ_{max} imply that a rough particle occupies excluded volumes larger than that of an equivalent ideal smooth sphere, especially in flow regimes where contacts are minimal and particles fully rotate in the flow field.

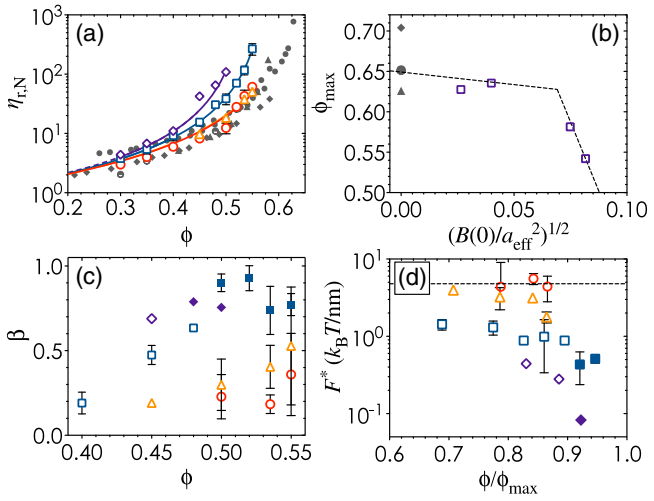

FIG. 3. Suspension properties as a function of roughness. (a) The relative quasi-Newtonian viscosity plotted against ϕ for smooth (red open circles), SL (orange open triangles), MR (blue open squares), and VR colloids (purple open diamonds). Solid lines are fits with the Eilers model. Gray solid symbols are literature data for sterically stabilized PMMA [21,42,43] and silica colloids [26]. (b) Maximum packing fraction plotted against rms roughness (open purple squares). Gray solid symbols are data of smooth colloids in literature [21,26,42,43]. Dashed lines guide the eye. (c) Shear thickening power for different ϕ. (d) Onset force F^* to push particles into contact. Dashed line indicates constant F^* for smooth colloids. In (c) and (d) the symbols follow the same legend as in (a). Solid symbols indicate flow curves for dilatant samples. Error bars represent standard deviation from three independent measurements where available.

Figure 3(b) plots ϕ_{max} as a function of roughness, along with values for smooth colloids from literature. When roughness is greater than a specific length scale $[B(\psi = 0)/a_{eff}^2)^{1/2} \geq 0.07a_{eff}]$, packing becomes increasingly difficult and, hence, the suspension viscosity diverges at a value of ϕ_{max} below that of the maximum random close packing of ideal spheres ($\phi_{max} = 0.64$). Interestingly, the value of ϕ_{max} for VR colloids ($\phi_{max} = 0.54$) is in agreement with the maximum packing reported for frictional particles [2,19].

Figure 3(b) supports our hypothesis that the rms roughness of particles needs to be sufficiently large in order for frictional contacts to be generated. This is likely due to the dissipative hydrodynamic forces from squeezing flow being diminished at a particle separation of $h = 0.07a_{eff}$ (Fig. S7 [35]). An analogous transition from the hydrodynamic to the boundary lubrication regime is well known in tribology [44] and granular packings. Studies of granular packings support our observation that ϕ_{max} decreases with increasing roughness, since frictional grains have a lower isostatic criterion [45].

Figure 3(c) shows that as roughness increases, there is a corresponding increase in the shear thickening power β. Based on our observations in Fig. 3(b), we hypothesize that tangential contributions from surface roughness can overcome the hydrodynamic forces that keep particles apart in quasi-Newtonian flow and in weak thickening. We estimate the force it takes to push two colloids into close contact using $F^* = \sigma_c a_{eff}^2$. It has been shown that the threshold stress scaling is $\sigma_c \sim a_{eff}^2$ for sterically stabilized PMMA particles, which comes from balancing the lubrication force and interparticle forces between the cross sectional area of a particle pair [15,21]. Figure 3(d) shows that $F^* = 4.7\ k_BT$/nm for smooth colloids at all ϕ/ϕ_{max}, consistent with the range of forces reported for PHSA-PMMA particles ($F^* = 2.4$–$6.0\ k_BT$/nm) [21,46]. These units represent the energy barrier that a pair of particles needs to overcome for a closer approach. Increasing surface roughness decreases F^* by nearly an order of magnitude. Plotting F^* against ϕ/ϕ_{max} does not collapse the data for different roughness, unlike studies in which the effect of repulsive interactions on the flow curve can be collapsed [33]. This suggests that there are other mechanisms in addition to packing effects during shear thickening and dilatancy. While granularlike frictional interactions and force networks may be present [47], elastohydrodynamic lubrication from particle deformation could also be present, although deformation is expected to reduce the thickening strength. The addition of the cross-linker in our synthesis procedure can result in an increase in the elastic modulus of PMMA by up to 40% at room temperature [48]. However, this change in modulus cannot immediately explain the observation of positive N_1 values [16]. Although the PHSA brush copolymer may entangle or adhere during flow [49,50], direct force measurements show that the interaction energy is purely repulsive down to a separation distance of ~5 nm [51]. Thus, the observed shear thickening behavior and the switch in the sign of N_1 from negative to positive is primarily due to the increasing roughness of the colloids. Future studies incorporating the second normal stress difference N_2 would be necessary to fully characterize the hydrodynamic interactions in dense suspensions [14,26].

According to Fig. 4, lubrication dominates the quasi-Newtonian flow of suspensions at low ϕ, σ, and roughness. When roughness increases, lubrication gradually gives way to other microscopic mechanisms that generate tangential forces and lower the critical stresses required for shear thickening and dilatancy. At the highest ϕ and σ, shear thickening and dilatancy are present because interparticle forces become sufficiently strong to deform particles or press them into solid-solid contact [6]. In the case of smooth colloids, the onset stress is constant up to $\phi = 0.55$. Roughness decreases the onset stress in a similar way to frictional interactions in granular materials, in which the microstructural criterion for mechanical stability is reduced [45,52].

Because friction is a major factor in dense suspensions, our work provides a guiding framework for predicting the rheology of a diverse class of colloidal materials with anisotropic particle shapes that introduce a hindered rotation mechanism in shear flow. Cornstarch is a particularly popular choice in studying jammed materials

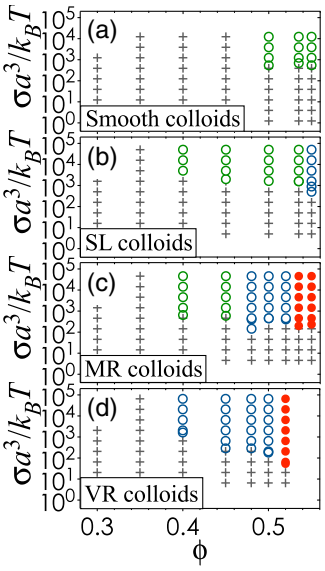

FIG. 4. Rheological state diagrams for rough colloids in sheared suspensions. (a)–(d) Transitions from quasi-Newtonian behavior to shear thickening and dilatancy are shown as a function of roughness. Gray crosses represent quasi-Newtonian flows ($\beta < 0.10$), green open circles represent weak thickening ($0.10 \leq \beta \leq 0.70$), blue open circles represent strong thickening ($0.70 \leq \beta \leq 1.0$), and red solid circles are dilatant flows ($N_1 > 0$).

[19,53,54]. However, individual granules possess irregularly faceted surfaces. Manipulation of particle roughness and shape represents a powerful tool for which the desired thickening response can be built into technology [55,56]. Moreover, researchers working on slurries can use particle roughness to minimize shear thickening or dilatancy.

We thank N. Wagner, J. Swan, W. Poon, D. Beltran-Villegas, S. Risbud, and A. Hollingsworth for advice and discussion. This work is supported in part by the National Science Foundation (NSF CBET No. 1232937, NSF CBET No. 1602183), a Rackham Predoctoral Fellowship (University of Michigan), and the US Army Research Office through a MURI grant (Award No. W911NF10-1-0518).

L. C. H. and S. J. contributed equally to this work.

*Corresponding author.
lilian_hsiao@ncsu.edu.
†Present address: National Renewable Energy Laboratory, Golden, Colorado 80401, USA

[1] N. J. Wagner and J. F. Brady, Phys. Today **62**, No. 10, 27 (2009).
[2] M. Wyart and M. E. Cates, Phys. Rev. Lett. **112**, 098302 (2014).
[3] Z. Pan, H. de Cagny, B. Weber, and D. Bonn, Phys. Rev. E **92**, 032202 (2015).
[4] V. T. O'Brien and M. E. Mackay, Langmuir **16**, 7931 (2000).
[5] E. Brown and H. M. Jaeger, Rep. Prog. Phys. **77**, 046602 (2014).
[6] J. R. Royer, D. L. Blair, and S. D. Hudson, Phys. Rev. Lett. **116**, 188301 (2016).
[7] O. Reynolds, Philos. Mag. Ser. 5 **20**, 469 (1885).
[8] M. Lee, M. Alcoutlabi, J. Magda, C. Dibble, M. Solomon, X. Shi, and G. McKenna, J. Rheol. **50**, 293 (2006).
[9] E. Brown and H. M. Jaeger, J. Rheol. **56**, 875 (2012).
[10] A. Fall, N. Huang, F. Bertrand, G. Ovarlez, and D. Bonn, Phys. Rev. Lett. **100**, 018301 (2008).
[11] X. Cheng, J. H. McCoy, J. N. Israelachvili, and I. Cohen, Science **333**, 1276 (2011).
[12] S. Jamali, M. Yamanoi, and J. Maia, Soft Matter **9**, 1506 (2013).
[13] D. R. Foss and J. F. Brady, J. Fluid Mech. **407**, 167 (2000).
[14] J. Bergenholtz, J. Brady, and M. Vicic, J. Fluid Mech. **456**, 239 (2002).
[15] J. Mewis and N. J. Wagner, *Colloidal Suspension Rheology* (Cambridge University Press, Cambridge, England, 2012).
[16] S. Jamali, A. Boromand, N. Wagner, and J. Maia, J. Rheol. **59**, 1377 (2015).
[17] A. K. Gurnon and N. J. Wagner, J. Fluid Mech. **769**, 242 (2015).
[18] R. Seto, R. Mari, J. F. Morris, and M. M. Denn, Phys. Rev. Lett. **111**, 218301 (2013).
[19] I. R. Peters, S. Majumdar, and H. M. Jaeger, Nature (London) **532**, 214 (2016).
[20] N. Y. C. Lin, B. M. Guy, M. Hermes, C. Ness, J. Sun, W. C. K. Poon, and I. Cohen, Phys. Rev. Lett. **115**, 228304 (2015).
[21] B. M. Guy, M. Hermes, and W. C. K. Poon, Phys. Rev. Lett. **115**, 088304 (2015).
[22] N. Fernandez, R. Mani, D. Rinaldi, D. Kadau, M. Mosquet, H. Lombois-Burger, J. Cayer-Barrioz, H. J. Herrmann, N. D. Spencer, and Lucio Isa, Phys. Rev. Lett. **111**, 108301 (2013).
[23] C. Heussinger, Phys. Rev. E **88**, 050201 (2013).
[24] R. Mari, R. Seto, J. F. Morris, and M. M. Denn, J. Rheol. **58**, 1693 (2014).
[25] D. Lootens, H. van Damme, Y. Hémar, and P. Hébraud, Phys. Rev. Lett. **95**, 268302 (2005).
[26] C. D. Cwalina and N. J. Wagner, J. Rheol. **58**, 949 (2014).
[27] L. Antl, J. Goodwin, R. Hill, R. H. Ottewill, S. Owens, S. Papworth, and J. Waters, Colloids Surf. **17**, 67 (1986).
[28] M. T. Elsesser and A. D. Hollingsworth, Langmuir **26**, 17989 (2010).
[29] L. Palangetic, K. Feldman, R. Schaller, R. Kalt, W. R. Caseri, and J. Vermant, Faraday Discuss. **191**, 325 (2016).
[30] L. C. Hsiao, R. S. Newman, S. C. Glotzer, and M. J. Solomon, Proc. Natl. Acad. Sci. U.S.A. **109**, 16029 (2012).
[31] J. Mewis and G. Biebaut, J. Rheol. **45**, 799 (2001).
[32] L.-N. Krishnamurthy, N. J. Wagner, and J. Mewis, J. Rheol. **49**, 1347 (2005).
[33] R. Mari, R. Seto, J. F. Morris, and M. M. Denn, Proc. Natl. Acad. Sci. U.S.A. **112**, 15326 (2015).
[34] S. Pednekar, J. Chun, and J. F. Morris, Soft Matter **13**, 1773 (2017).
[35] See Supplemental Material at http://link.aps.org/supplemental/10.1103/PhysRevLett.119.158001 for specific details.

[36] D. Kim, D. Y. Lee, K. Lee, and S. Choe, Macromol. Res. **17**, 250.
[37] W. C. K. Poon, E. R. Weeks, and C. P. Royall, Soft Matter **8**, 21 (2012).
[38] J. M. Bennett, Appl. Opt. **15**, 2705 (1976).
[39] B. J. Maranzano and N. J. Wagner, J. Chem. Phys. **114**, 10514 (2001).
[40] J. J. Stickel and R. L. Powell, Annu. Rev. Fluid Mech. **37**, 129 (2005).
[41] D. B. Genovese, Adv. Colloid Interface Sci. **171–172**, 1 (2012).
[42] S.-E. Phan, W. B. Russel, Z. Cheng, J. Zhu, P. M. Chaikin, J. H. Dunsmuir, and R. H. Ottewill, Phys. Rev. E **54**, 6633 (1996).
[43] W. J. Frith, P. d'Haene, R. Buscall, and J. Mewis, J. Rheol. **40**, 531 (1996).
[44] G. Stachowiak and A. W. Batchelor, *Engineering Tribology* (Butterworth-Heinemann, London, 2013).
[45] M. v. Hecke, J. Phys. Condens. Matter **22**, 033101 (2010).
[46] G. Bryant, S. R. Williams, L. Qian, I. K. Snook, E. Perez, and F. Pincet, Phys. Rev. E **66**, 060501 (2002).
[47] D. Bi, J. Zhang, B. Chakraborty, and R. P. Behringer, Nature (London) **480**, 355 (2011).
[48] K. Tamareselvy and F. A. Rueggeberg, Dental materials **11**, 265 (1995).
[49] S. Auer, W. C. K. Poon, and D. Frenkel, Phys. Rev. E **67**, 020401 (2003).
[50] D. Cebula, J. Goodwin, R. H. Ottewill, G. Jenkin, and J. Tabony, Colloid Polym. Sci. **261**, 555 (1983).
[51] B. Costello, P. Luckham, and T. F. Tadros, Langmuir **8**, 464 (1992).
[52] L. E. Silbert, Soft Matter **6**, 2918 (2010).
[53] A. Fall, F. Bertrand, D. Hautemayou, C. Mezière, P. Moucheront, A. Lemaítre, and G. Ovarlez, Phys. Rev. Lett. **114**, 098301 (2015).
[54] Y. Madraki, S. Hormozi, G. Ovarlez, E. Guazzelli, and O. Pouliquen, Phys. Rev. Fluids **2**, 033301 (2017).
[55] Y. S. Lee, E. D. Wetzel, and N. J. Wagner, J. Mater. Sci. **38**, 2825 (2003).
[56] E. Brown, N. Rodenberg, J. Amend, A. Mozeika, E. Steltz, M. R. Zakin, H. Lipson, and H. M. Jaeger, Proc. Natl. Acad. Sci. U.S.A. **107**, 18809 (2010).